

Buckling analysis of functionally graded hybrid composite plates using a new four variable refined plate theory

A. Fekrar¹, N. El Meiche¹, A. Bessaim¹, A. Tounsi^{*1,2}, and E. A. Adda Bedia¹

¹Laboratoire des Matériaux et Hydrologie, Université de Sidi Bel Abbès, Algérie

²Département de Génie Civil, Faculté des Sciences de L'Ingénieur, Université de Sidi Bel Abbès, Algérie

(Received February 26, 2012, Revised April 18, 2012, Accepted May 01, 2012)

Abstract. In this research, mechanical buckling of hybrid functionally graded plates is considered using a new four variable refined plate theory. Unlike any other theory, the number of unknown functions involved is only four, as against five in case of other shear deformation theories. The theory presented is variationally consistent, does not require shear correction factor, and gives rise to transverse shear stress variation such that the transverse shear stresses vary parabolically across the thickness satisfying shear stress free surface conditions. The plate properties are assumed to be varied through the thickness following a simple power law distribution in terms of volume fraction of material constituents. Governing equations are derived from the principle of minimum total potential energy. The closed-form solution of a simply supported rectangular plate subjected to in-plane loading has been obtained by using the Navier method. The effectiveness of the theories is brought out through illustrative examples.

Keywords: plate theory; buckling analysis; functionally graded materials.

1. Introduction

Functionally graded materials (FGM) had been utilized in the aerospace and other industries in recent years because of their superior heat-shielding properties. The functionally graded material for high-temperature applications may be composed of ceramic and metal. The surface of a ceramic exposed to high temperature due to its low thermal conductivity. The material properties of functionally graded material vary continuously along certain dimension of the structure, but that of the fiber-reinforced laminated composite materials are discontinuous across adjoining layers which result in the delaminating mode of failure.

In recent years, researches on FGM plates have received great attention, and a variety of plate theories has been introduced based on considering the transverse shear deformation effect. In company with studies of buckling behavior of plate, many plate theories have been developed. The Classic Plate Theory (CPT) provides a theoretical model of plate behavior which has some considerable advantages, which can be employed with confidence over a reasonable range of applications, but which also has significant limitations. The popularity of CPT arises from the fact that the bending behavior of a plate is expressed in terms of a sole, fundamental reference quantity that is w , the lateral displacement of the

* Corresponding author, Professor, E-mail: tou_abdel@yahoo.com

middle surface. The Kirchhoff hypothesis is used in CPT that straight lines originally normal to the plate middle surface remain straight and normal during the deformation process. The consequence of using this hypothesis is that the effect of through-thickness shear deformation is ignored in CPT and thus the classical theory overestimates the stiffness of the plate. Such overestimation is of little consequence for truly thin plates but can be of very considerable significance for other plates, particularly in vibration and buckling problems when the ratio of plate thickness to typical wavelength increases. This theory was employed for buckling analysis of FGM plate by Feldman and Aboudi (1997), Javaheri and Eslami (2002), Abrate (2008), Mahdavian (2009), and Mohammadi *et al.* (2010). However, it underpredicts deflections and overpredicts frequencies as well as buckling loads of moderately thick plate (Reddy 2004). A number of plate theories exist in which the Kirchhoff hypothesis is relaxed to take account of shear deformation and related effects and amongst these theories, those of Mindlin (1951) and Reissner (1945) are closely related and are well known. The Mindlin (1951) and Reissner (1945) theories are known as the first-order shear deformable theory (FSDT), and account for the transverse shear effects by the way of linear variation of in-plane displacements through the thickness. Many studies of the buckling analysis of FGM plate have been carried out using FSDT (Shariat and Eslami 2005, Yang *et al.* 2005, Zhao *et al.* 2009, Bouazza *et al.* 2010). However, these models do not satisfy the zero traction boundary conditions on the top and bottom faces of the plate, and need to use the shear correction factor to satisfy the constitutive relations for transverse shear stresses and shear strains. For these reasons, many higher-order theories have been developed to improve in FSDT such as Levinson (1980) and Reddy (1984). Indeed, Reddy (1984) put forward a parabolic shear deformation theory (PSDT) which considers not only the transverse shear strains, but also their parabolic variation across the plate thickness. Although different plate theories have been adopted for buckling analysis of FGM plates, buckling of ceramic-FGM-metal plates has not been seen in the literature.

In this paper, a new four variable refined plate theory involving only four unknown functions, as against five functions in case of Reissner's and Mindlin's theories is developed for the buckling behavior of ceramic-FGM-metal plate subjected to the in-plane loading. Using the Navier method, the closed-form solutions have been obtained to analyze its buckling behaviors. The effects of various variables, such as FGM layer thickness, volume fraction index, layer thickness ratio, thickness ratio, and aspect ratio, on the critical buckling load of hybrid FGM plates are investigated and discussed.

2. Modeling of functionally graded material

A hybrid functionally graded plate with uniform thickness h , which is made of ceramics and metals, is considered in this study. Similar to a sandwich laminate plate, the ceramic-FGM-metal plate consists of three layers, a top layer of all-ceramic material ($h/2 \sim z_C$), a core layer of all-FGM material ($z_C \sim -z_M$) and a bottom layer of all-metal material ($-z_M \sim -h/2$). The FGM layer is also made of ceramic and metal, in which the ceramic volume fraction varies from 0% at the interface between the pure-metal layer and FGM to 100% at the interface between the FGM and pure-ceramic layer. A number of micromechanics models that have been proposed for the determination of effective properties of FGMs based on the rule of mixture called by the Voigt model (Gibson *et al.* 1995), Mori-Tanaka scheme (Mori and Tanaka 1973) and self-consistent method (Hill 1965). The Mori-Tanaka model is applicable to a discontinuous particulate phase, whereas the Voigt model is simple and convenient to apply for predicting the overall material properties and responses of the structures. However, Chehel Amirani *et al.* (2009) have showed that there is insignificant difference between the results obtained by these two

techniques (Mori-Tanaka model and the rule of mixtures technique). Consequently, the Voigt model is reasonable for predicting the global responses of the FGM structures.

Using the Voigt model (Gibson *et al.* 1995), Young’s modulus E of an FGM layer of the functionally graded plate are assumed as

$$E(z) = E_C V_C + E_M V_M = E_C V_C + E_M(1 - V_C) \tag{1}$$

here, E_C and E_M are the elastic modulus of the ceramic and metal, respectively. V_C is the volume fraction of the ceramic and is expressed by a simple power law as follows

$$V_C = \left(\frac{2z + h}{2h} \right)^p \tag{2}$$

where the non-negative exponent p is called volume fraction index; z is the thickness coordinate variable, $-z_M \leq z \leq z_C$. By substituting Eq. (2) into (1), the material properties of an FGM layer can be expressed as

$$E(z) = (E_C - E_M) \left(\frac{2z + h}{2h} \right)^p + E_M \tag{3}$$

Eq. (3) can be used to determine Young’s modulus E of a ceramic-FGM-metal plate at any position. However, Poisson’s ratio (ν) is assumed to be constant because there is small change in value between ceramic and metal; therefore, the average value can be used for calculation. Indeed, Delale and Erdogan (1983) indicated that the effect of Poisson’s ratio on the deformation is much less than that of Young’s modulus. Thus, Poisson’s ratio of the plates is assumed to be constant. The study of its effect on the static response of the plate can be found in Chi and Chung (2006a, b).

Fig. 1 depicts the variation of ceramic volume fraction through the thickness of ceramic-FGM-metal plate. The ceramic-FGM-metal plate consists of a top layer of all-ceramic material ($h/2 \sim z_C$), a middle layer of all-FGM material ($z_C \sim -z_M$) and a bottom layer of all-metal material ($-z_M \sim -h/2$). The volume fraction index p is set to be 0.1, 0.2, 0.5, 1, 2, 5 and 10. The y -axis of the figure stands for the volumetric

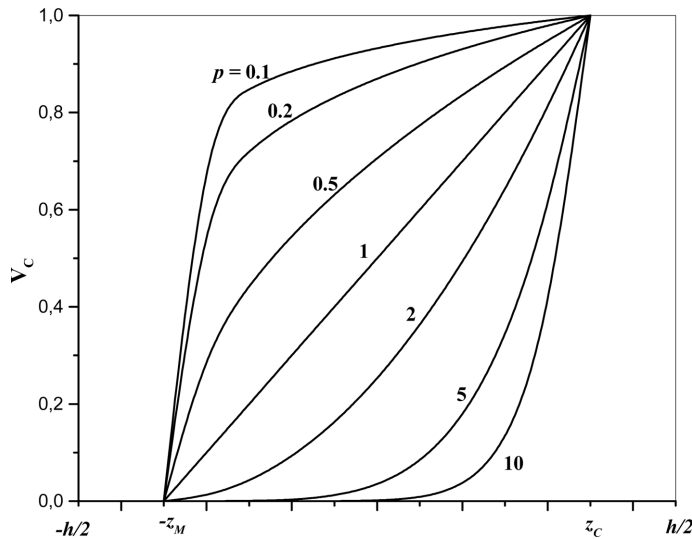


Fig. 1 Variation of ceramic volume fraction along the thickness of the functionally graded plate

percentage of ceramic, while the x -axis represents the position along the thickness of ceramic-FGM-metal plate. It can be observed in Fig. 1 that the ceramic volume fraction ranges from 0% to 100% in the FGM layer. A small value of volume fraction index, p , gives a rapid increase of the ceramic constituent at the interface of pure-metal and ceramic layers.

3. Present new four variable refined plate theory

3.1 Assumptions of the present plate theory

Assumptions of the present theory are as follows:

- (i) The displacements are small in comparison with the plate thickness and, therefore, strains involved are infinitesimal.
- (ii) The transverse displacement w includes two components of bending w_b , and shear w_s . These components are functions of coordinates x, y only.

$$w(x, y, z) = w_b(x, y) + w_s(x, y) \quad (4)$$

- (iii) The transverse normal stress σ_z is negligible in comparison with in-plane stresses σ_x and σ_y .
- (iv) The displacements u in x -direction and v in y -direction consist of extension, bending, and shear components.

$$u = u_0 + u_b + u_s, \quad v = v_0 + v_b + v_s \quad (5)$$

The bending components u_b and v_b are assumed to be similar to the displacements given by the classical plate theory. Therefore, the expression for u_b and v_b can be given as

$$u_b = -z \frac{\partial w_b}{\partial x}, \quad v_b = -z \frac{\partial w_b}{\partial y} \quad (6)$$

The shear components u_s and v_s give rise, in conjunction with w_s , to the parabolic variations of shear strains γ_{xz} , γ_{yz} and hence to shear stresses τ_{xz} , τ_{yz} through the thickness of the plate in such a way that shear stresses τ_{xz} , τ_{yz} are zero at the top and bottom faces of the plate. Consequently, the expression for u_s and v_s can be given as

$$u_s = -f(z) \frac{\partial w_s}{\partial x}, \quad v_s = -f(z) \frac{\partial w_s}{\partial y} \quad (7)$$

3.2 Kinematics and governing equations

Based on the assumptions made in the preceding section, the displacement field can be obtained using Eqs. (4)-(7) as

$$u(x, y, z) = u_0(x, y) - z \frac{\partial w_b}{\partial x} - f(z) \frac{\partial w_s}{\partial x} \quad (8a)$$

$$v(x, y, z) = v_0(x, y) - z \frac{\partial w_b}{\partial y} - f(z) \frac{\partial w_s}{\partial y}$$

$$w(x, y, z) = w_b(x, y) + w_s(x, y)$$

where

$$f(z) = z \left[1 + \frac{3\pi}{2} \operatorname{sech}^2 \left(\frac{1}{2} \right) \right] - \frac{3\pi}{2} h \tanh \left(\frac{z}{h} \right) \quad (8b)$$

The strains associated with the displacements in Eq. (8) are

$$\begin{aligned} \varepsilon_x &= \varepsilon_x^0 + zk_x^b + f(z)k_x^s \\ \varepsilon_y &= \varepsilon_y^0 + zk_y^b + f(z)k_y^s \\ \gamma_{xy} &= \gamma_{xy}^0 + zk_{xy}^b + f(z)k_{xy}^s \\ \gamma_{yz} &= g(z)\gamma_{yz}^s \\ \gamma_{xz} &= g(z)\gamma_{xz}^s \\ \varepsilon_z &= 0 \end{aligned} \quad (9)$$

where

$$\begin{aligned} \varepsilon_x^0 &= \frac{\partial u_0}{\partial x}, \quad k_x^b = -\frac{\partial^2 w_b}{\partial x^2}, \quad k_x^s = -\frac{\partial^2 w_s}{\partial x^2} \\ \varepsilon_y^0 &= \frac{\partial v_0}{\partial y}, \quad k_y^b = -\frac{\partial^2 w_b}{\partial y^2}, \quad k_y^s = -\frac{\partial^2 w_s}{\partial y^2} \\ \gamma_{xy}^0 &= \frac{\partial u_0}{\partial y} + \frac{\partial v_0}{\partial x}, \quad k_{xy}^b = -2\frac{\partial^2 w_b}{\partial x \partial y}, \quad k_{xy}^s = -2\frac{\partial^2 w_s}{\partial x \partial y} \\ \gamma_{yz}^s &= \frac{\partial w_s}{\partial y}, \quad \gamma_{xz}^s = \frac{\partial w_s}{\partial x}, \quad g(z) = 1 - f'(z) \quad \text{and} \quad f'(z) = \frac{df(z)}{dz} \end{aligned} \quad (10)$$

The constitutive law including the thermal effect can be written in the following form

$$\begin{Bmatrix} \sigma_x \\ \sigma_y \\ \tau_{yz} \\ \tau_{xz} \\ \tau_{xy} \end{Bmatrix} = \begin{bmatrix} Q_{11} & Q_{12} & 0 & 0 & 0 \\ Q_{12} & Q_{22} & 0 & 0 & 0 \\ 0 & 0 & Q_{44} & 0 & 0 \\ 0 & 0 & 0 & Q_{55} & 0 \\ 0 & 0 & 0 & 0 & Q_{66} \end{bmatrix} \begin{Bmatrix} \varepsilon_x \\ \varepsilon_y \\ \gamma_{yz} \\ \gamma_{xz} \\ \gamma_{xy} \end{Bmatrix} \quad (11)$$

where $(\sigma_x, \sigma_y, \tau_{xy}, \tau_{yz}, \tau_{yx})$ and $(\varepsilon_x, \varepsilon_y, \gamma_{xy}, \gamma_{yz}, \gamma_{yx})$ are the stress and strain components, respectively. Using the material properties defined in Eq. (3), stiffness coefficients, Q_{ij} , can be expressed as

$$Q_{11} = Q_{22} = \frac{E(z)}{1 - \nu^2} \quad (12a)$$

$$Q_{12} = \frac{\nu E(z)}{1 - \nu^2} \quad (12b)$$

$$Q_{44} = Q_{55} = Q_{66} = \frac{E(z)}{2(1 + \nu)} \quad (12c)$$

The governing equations can be obtained by using the principle of minimum total potential energy and the four governing equations are given as follows

$$A_{11}d_{11}u_0 + A_{66}d_{22}u_0 + (A_{12} + A_{66})d_{12}v_0 - B_{11}d_{111}w_b - (B_{12} + 2B_{66})d_{122}w_b \quad (13a)$$

$$- (B_{12}^s + 2B_{66}^s)d_{122}w_s - B_{11}^s d_{111}w_s = 0$$

$$A_{22}d_{22}v_0 + A_{66}d_{11}v_0 + (A_{12} + A_{66})d_{12}u_0 - B_{22}d_{222}w_b - (B_{12} + 2B_{66})d_{112}w_b \quad (13b)$$

$$- (B_{12}^s + 2B_{66}^s)d_{112}w_s - B_{22}^s d_{222}w_s = 0$$

$$B_{11}d_{111}u_0 + (B_{12} + 2B_{66})d_{122}u_0 + (B_{12} + 2B_{66})d_{112}v_0 + B_{22}d_{222}v_0 - D_{11}d_{1111}w_b \quad (13c)$$

$$- 2(D_{12} + 2D_{66})d_{1122}w_b - D_{22}d_{2222}w_b - D_{11}^s d_{1111}w_s - 2(D_{12}^s + 2D_{66}^s)d_{1122}w_s - D_{22}^s d_{2222}w_s + \bar{N} = 0$$

$$B_{11}^s d_{111}u_0 + (B_{12}^s + 2B_{66}^s)d_{122}u_0 + (B_{12}^s + 2B_{66}^s)d_{112}v_0 + B_{22}^s d_{222}v_0 - D_{11}^s d_{1111}w_b \quad (13e)$$

$$- 2(D_{12}^s + 2D_{66}^s)d_{1122}w_b - D_{22}^s d_{2222}w_b - H_{11}^s d_{1111}w_s - 2(H_{12}^s + 2H_{66}^s)d_{1122}w_s$$

$$- H_{22}^s d_{2222}w_s + A_{55}^s d_{11}w_s + A_{44}^s d_{22}w_s + \bar{N} = 0$$

where d_{ij} , d_{ijl} and d_{ijlm} are the following differential operators

$$d_{ij} = \frac{\partial^2}{\partial x_i \partial x_j}, \quad d_{ijl} = \frac{\partial^3}{\partial x_i \partial x_j \partial x_l}, \quad d_{ijlm} = \frac{\partial^4}{\partial x_i \partial x_j \partial x_l \partial x_m}, \quad (i, j, l, m = 1, 2) \quad (14)$$

and

$$\bar{N} = \left[N_x^0 \frac{\partial^2 (w_b + w_s)}{\partial x^2} + N_y^0 \frac{\partial^2 (w_b + w_s)}{\partial y^2} + 2N_{xy}^0 \frac{\partial^2 (w_b + w_s)}{\partial x \partial y} \right] \quad (15)$$

where N_m^0 , N_y^0 and N_{xy}^0 are in-plane pre-buckling forces.

The coefficients in the governing equations associated with material parameters of hybrid functionally graded plates are defined as

$$\left\{ \begin{array}{cccccc} A_{11} & B_{11} & D_{11} & B_{11}^s & D_{11}^s & H_{11}^s \\ A_{12} & B_{12} & D_{12} & B_{12}^s & D_{12}^s & H_{12}^s \\ A_{66} & B_{66} & D_{66} & B_{66}^s & D_{66}^s & H_{66}^s \end{array} \right\} = \int_{-h/2}^{h/2} Q_{11}(1, z, z^2, f(z), zf(z), f^2(z)) \left\{ \begin{array}{c} 1 \\ \nu \\ \frac{1-\nu}{2} \end{array} \right\} dz \quad (16a)$$

and

$$(A_{22}, B_{22}, D_{22}, B_{22}^s, D_{22}^s, H_{22}^s) = (A_{11}, B_{11}, D_{11}, B_{11}^s, D_{11}^s, H_{11}^s) \quad (16b)$$

$$A_{44}^s = A_{55}^s = \int_{-h/2}^{h/2} \frac{E(z)}{2(1+\nu)} [g(z)]^2 dz \quad (16c)$$

Clearly, when the effect of transverse shear deformation is neglected ($w_s = 0$), the governing equation Eq. (13) yields the governing equation of hybrid FGM plate based on the classical plate theory.

4. Buckling analysis

4.1 Navier solution for simply supported rectangular plates

Consider a simply supported rectangular ceramic-FGM-metal plate with length a and width b and subjected to an in-plane loading in two directions ($N_x^0 = \gamma_1 N_{cr}$, $N_y^0 = \gamma_2 N_{cr}$, $N_{xy}^0 = 0$) as shown in Fig. 2. The simply supported boundary conditions are given as follows

$$v_0 = w_b = w_s = \frac{\partial w_s}{\partial y} = N_x = M_x^b = M_x^s = 0 \quad \text{on edges } x=0, a \quad (17a)$$

$$u_0 = w_b = w_s = \frac{\partial w_s}{\partial x} = N_y = M_y^b = M_y^s = 0 \quad \text{on edges } y=0, b \quad (17b)$$

The displacement functions that satisfy the equations of boundary conditions (17) are selected as the following Fourier series

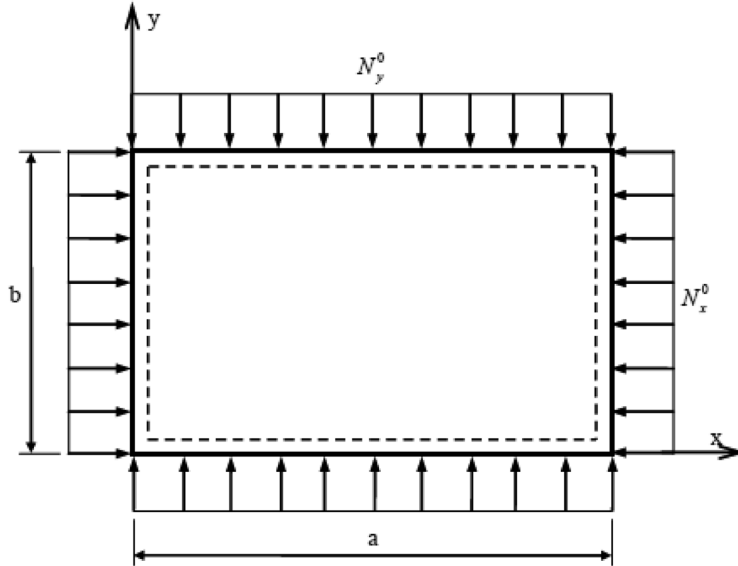


Fig. 2 Rectangular plate subjected to in-plane loading

$$\begin{Bmatrix} u_0 \\ v_0 \\ w_b \\ w_s \end{Bmatrix} = \sum_{m=1}^{\infty} \sum_{n=1}^{\infty} \begin{Bmatrix} U_{mn} \cos(\lambda x) \sin(\mu y) \\ V_{mn} \sin(\lambda x) \cos(\mu y) \\ W_{bmn} \sin(\lambda x) \cos(\mu y) \\ W_{smn} \sin(\lambda x) \sin(\mu y) \end{Bmatrix} \quad (18)$$

where U_{mn} , V_{mn} , W_{bmn} , and W_{smn} are arbitrary parameters to be determined and $\lambda = m\pi/a$ and $\mu = n\pi/b$. Substituting Eq. (18) into Eq. (13), the closed-form solution of buckling load N_{cr} can be determined from the following eigenvalue equation

$$\begin{bmatrix} a_{11} & a_{12} & a_{13} & a_{14} \\ a_{12} & a_{22} & a_{23} & a_{24} \\ a_{13} & a_{23} & a_{33} + k & a_{34} + k \\ a_{14} & a_{24} & a_{34} + k & a_{44} + k \end{bmatrix} \begin{Bmatrix} U_{mn} \\ V_{mn} \\ W_{bmn} \\ W_{smn} \end{Bmatrix} = \begin{Bmatrix} 0 \\ 0 \\ 0 \\ 0 \end{Bmatrix} \quad (19)$$

where

$$\begin{aligned} a_{11} &= A_{11}\lambda^2 + A_{66}\mu^2 \\ a_{12} &= \lambda\mu(A_{12} + A_{66}) \\ a_{13} &= -\lambda[B_{11}\lambda^2 + (B_{12} + 2B_{66})\mu^2] \\ a_{14} &= -\lambda[B_{11}^s\lambda^2 + (B_{12}^s + 2B_{66}^s)\mu^2] \\ a_{22} &= A_{66}\lambda^2 + A_{22}\mu^2 \\ a_{23} &= -\mu[(B_{12} + 2B_{66})\lambda^2 + B_{22}\mu^2] \\ a_{24} &= -\mu[(B_{12}^s + 2B_{66}^s)\lambda^2 + B_{22}^s\mu^2] \\ a_{33} &= D_{11}\lambda^4 + 2(D_{12} + 2D_{66})\lambda^2\mu^2 + D_{22}\mu^4 \\ a_{34} &= D_{11}^s\lambda^4 + 2(D_{12}^s + 2D_{66}^s)\lambda^2\mu^2 + D_{22}^s\mu^4 \\ a_{44} &= H_{11}^s\lambda^4 + 2(H_{12}^s + 2H_{66}^s)\lambda^2\mu^2 + H_{22}^s\mu^4 + A_{55}^s\lambda^2 + A_{44}^s\mu^2 \\ k &= N_{cr}(\gamma_1\mu^2 + \gamma_2\lambda^2) \end{aligned} \quad (20)$$

By applying the static condensation approach we obtained the expression of buckling load

$$N_{cr} = \frac{-1}{\gamma_1\mu^2 + \gamma_2\lambda^2} \frac{\bar{a}_{33}\bar{a}_{44} - \bar{a}_{34}\bar{a}_{43}}{\bar{a}_{33} + \bar{a}_{44} - \bar{a}_{34} - \bar{a}_{43}} \quad (21)$$

where

$$\bar{a}_{33} = a_{33} - a_{13} \frac{b_1}{b_0} - a_{23} \frac{b_2}{b_0}, \quad \bar{a}_{34} = a_{34} - a_{14} \frac{b_1}{b_0} - a_{24} \frac{b_2}{b_0} \quad (22)$$

$$\bar{a}_{43} = a_{34} - a_{13} \frac{b_3}{b_0} - a_{23} \frac{b_4}{b_0}, \quad \bar{a}_{44} = a_{44} - a_{14} \frac{b_3}{b_0} - a_{24} \frac{b_4}{b_0}$$

$$b_0 = a_{11}a_{12} - a_{12}^2, \quad b_1 = a_{13}a_{22} - a_{12}a_{23}, \quad b_2 = a_{11}a_{23} - a_{12}a_{13}$$

$$b_3 = a_{14}a_{22} - a_{12}a_{24}, \quad b_4 = a_{11}a_{24} - a_{12}a_{14}$$

For the case of CPT, the expression of buckling load N_{cr} can be simplified by setting the shear component of transverse displacement to zero ($w_s = 0$) as

$$N_{cr} = \frac{-\bar{a}_{33}}{\gamma_1 \mu^2 + \gamma_2 \lambda^2} \quad (23)$$

For each choice of m and n , there is a corresponsive unique value of N_{cr} . The critical buckling load is the smallest value of $N_{cr}(m, n)$.

4.2 The Ritz solution of the buckling problem of FGM plates with various boundary conditions

In applying Ritz method, the displacement components are assumed as infinite series forms of the unknown functions depending on the lateral coordinates of the plate. By taking a sufficient number of terms in these series, it is possible to approach the exact solution of the problem considered. Although different unknown functions can be chosen, in this study, after defining nondimensional coordinates as $\xi = 2x/a$ and $\eta = 2y/b$ choosing the origin of the coordinates as $-1 \leq \xi \leq 1$ and $-1 \leq \eta \leq 1$, and, we will assume the displacement components as the following the simple algebraic polynomials which are the power functions of coordinate parameters in the expansion of double infinite series

$$(u_0, v_0, w_b, w_s) = \sum_{f=0}^{F-1} \sum_{g=0}^{G-1} (U_{ij}, V_{kl}, C_{mn}, E_{pq}) X_f(\xi) Y_g(\eta) \quad (24)$$

where the polynomials are defined as

$$X_f(\xi) = \xi^f (\xi + 1)^{B_1} (\xi - 1)^{B_3}, \quad f = i, k, m, p \quad (25a)$$

$$Y_g(\eta) = \eta^g (\eta + 1)^{B_2} (\eta - 1)^{B_4} \quad g = j, l, n, q \quad (25b)$$

and U_{ij}, V_{kl}, C_{mn} and E_{pq} are unknown constant coefficients. Here, B_i 's can take the values of 0, 1 and 2 corresponding to the free, simply supported and clamped edges, respectively (Narita 2000). The 'i' subindices of B_i 's denote the number of the subsequent edges of the plate in the counter clockwise direction where the edge numbered as 1 is at $\xi = -1$. It should be remembered that Ritz method satisfies only the geometric boundary conditions, it is possible to satisfy any sets of geometric edge boundary condition required. The boundary conditions along the edges of the plate presented in Table 1 will be

considered in this study.

Upon inserting the displacement forms (Eq. (24)) into the strain energy and potential energy of in-plane loads and after minimizing the functional of the total potential energy of the plate with respect to the coefficients of the displacement functions, a system of algebraic simultaneous equations with the same number of unknown coefficients of Eq. (24) is obtained. The number of these equations is $5M^2$ if the same number of terms is taken in all of the series ($F = G = M$). The algebraic equations are given as follows in the form of the generalized eigenvalue problem

$$|K - \bar{N}M|X = 0 \quad (26)$$

where \bar{N} is the buckling load parameter, K and M are stiffness and geometry matrices, respectively, and X contains the unknown coefficients of the series (24). For a non-trivial solution, the eigenvalues (\bar{N}) which make the determinant to be equal to zero, correspond to the critical buckling loads.

5. Results and discussion

In this section, buckling analysis of simply supported rectangular ceramic-FGM-metal plates by the formulation presented above is investigated. The ceramic-FGM-metal plates are subjected to different types of in-plane loading. The total thickness of the ceramic-FGM-metal plate is h , where $h = t_{Ceramic} + t_{FGM} + t_{Metal}$. $t_{Ceramic}$, t_{FGM} and t_{Metal} are the layer thickness of pure ceramic, all-FGM and pure metal, respectively. In the following analysis, an FGM with two constituent materials, Aluminum and Silicon Carbide, is investigated. The Young's modulus for Silicon Carbide is $E_C = 420$ GPa and for Aluminum is $E_M = 70$ GPa, respectively. Note that, Poisson's ratio is selected constant for both Aluminum and Silicon Carbide and it equal to 0.3.

To verify the accuracy of present theory, comparison is made between the results obtained from the present model and those of Bodaghi and Saidi (2010) based on higher shear deformation theory (HSDT) as given in Table 2. The critical buckling loads of all-FGM plate ($t_{FGM}/h = 1$) for variation of side-to-thickness ratio, aspect ratio, and power of FGM are shown in Table 1. It can be seen that the present results are in agreement with the published results. It should be noted that the unknown function in present theory is four, while the unknown function in HSDT is five. It can be concluded that the present theory is not only accurate but also simple in predicting critical buckling load of FGM plates.

Table 1 The kinematic edge boundary conditions of the plates considered

	Boundary condition type	
	At $\xi = \pm 1$	At $\eta = \pm 1$
Simply supported (S)	$v_0 = w_b = w_s = \partial w_s / \partial \eta = 0$	$u_0 = w_b = w_s = \partial w_s / \partial \xi = 0$
Clamped (C)	$u_0 = v_0 = w_b = w_s = \partial w_b / \partial \xi = \partial w_s / \partial \xi = \partial w_s / \partial \eta = 0$	$u_0 = v_0 = w_b = w_s = \partial w_b / \partial \eta = \partial w_s / \partial \xi = \partial w_s / \partial \eta = 0$
Free (F)	$u_0 \neq 0, v_0 \neq 0, w_b \neq 0, w_s \neq 0, \partial w_s / \partial \xi \neq 0, \partial w_s / \partial \eta \neq 0$ (no constraints)	$u_0 \neq 0, v_0 \neq 0, w_b \neq 0, w_s \neq 0, \partial w_s / \partial \xi \neq 0, \partial w_s / \partial \eta \neq 0$ (no constraints)

Table 2 Comparison of critical buckling load N_{cr} (MN/m) of rectangular all-FGM plate

(γ_1, γ_2)	a/b	a/h	Theory	P		
				0	1	2
(-1,0)	0.5	10	Present	2080.010	1028.554	780.149
			HSDT**	2079,721	1028,412	780,097
		5	Present	12172.770	6275.972	4695.067
			HSDT**	12162,119	6270,298	4692,542
	1	10	Present	1437.452	702.276	534.807
			HSDT**	1437,361	702,304	534,441
		5	Present	9918.275	4956.375	3746.287
			HSDT**	9915,620	4955,431	3746,054
	1.5	10	Present	1528.089 ^a	749.027 ^a	569.786 ^a
			HSDT**	1527,903 ^a	748,92 ^a	569,751 ^a
		5	Present	10048.091 ^a	5069.449 ^a	3819.647 ^a
			HSDT**	10044,721 ^a	5067,219 ^a	3819,109 ^a
(-1,-1)	0.5	10	Present	1664.008	822.843	624.119
			HSDT**	1663,777	822,738	624,158
		5	Present	9738.216	5020.777	3756.054
			HSDT**	9729,999	5016,384	3754,274
	1	10	Present	718.726	351.138	267.403
			HSDT**	718,692	351,124	267,416
		5	Present	4959.137	2478.187	1873.143
			HSDT**	4957,888	2477,589	1873,19
	1.5	10	Present	526.878	256.782	195.706
			HSDT**	526,861	256,776	195,714
		5	Present	3773.504	1871.329	1418.040
			HSDT**	3772,877	1871,038	1418,12
(-1,1)	0.5	10	Present	2773.347	1371.406	1040.199
			HSDT**	2772,98	1371,653	1040,519
		5	Present	16230.36	8367.962	6260.09
			HSDT**	16216,712	8360,541	6257,811
	1	10	Present	2773.347 ^a	1371.406 ^a	1040.199 ^a
			HSDT**	2772,98 ^a	1371,653 ^a	1040,519 ^a
		5	Present	16230.360 ^a	8367.962 ^a	6260.090 ^a
			HSDT**	16216,712 ^a	8360,541 ^a	6257,811 ^a
	1.5	10	Present	2773.347 ^b	1371.406 ^b	1040.199 ^b
			HSDT**	2772,98 ^b	1371,653 ^b	1040,519 ^b
		5	Present	16223.643 ^b	8360.414 ^b	6257.811 ^b
			HSDT**	16216,712 ^b	8360,541 ^b	6257,811 ^b

^aMode for plate is (m, n) = (2, 1); ^bMode for plate is (m, n) = (3, 1)

**Bodaghi and Saidi 2010

In Table 3, the non-dimensional critical buckling loads are presented in order to compare with those given by Mohammadi *et al.* (2010b) based on FSDT and Bodaghi and Saidi (2010) based on HSDT for

Table 3 Comparison of nondimensional critical buckling load of square FGM plate with different boundary conditions ($a/h = 10$)

(γ_1, γ_2)	p	Theory	Boundary conditions					
			SCSC	SSSC	SSSS	SFSC	SSSF	SFSF
(-1,0)	0	Present	63.7145	51.5323	37.3719	15.5186	13.2820	9.1321
		HSDT*	63.1628	51.5934	37.3714	15.4545	13.2503	9.1224
		FSDT**	63.0039	51.5506	37.3708	15.3653	13.2384	9.1020
	1	Present	65.1987	52.2819	37.7154	15.6892	13.3934	9.1730
		HSDT*	64.9643	52.3717	37.7172	15.5703	13.3634	9.1601
		FSDT**	64.8195	52.3414	37.7132	15.4950	13.3221	9.1469
	2	Present	65.0122	52.4011	37.5915	15.5012	13.2217	9.1521
		HSDT*	64.3779	52.1168	37.5765	15.2934	13.1840	9.1089
		FSDT**	64.7963	52.3314	37.7089	15.4933	12.2483	9.1464
(-1,-1)	0	Present	33.4847	24.2261	18.6862	10.6152	9.9878	8.8851
		HSDT*	33.3392	24.1989	18.6860	10.5061	9.8265	8.8613
		FSDT**	33.3206	24.1927	18.6854	10.5027	9.8243	8.8604
	1	Present	34.2784	24.6215	18.8573	10.7133	10.0238	8.9712
		HSDT*	34.0121	24.5260	18.8571	10.5997	9.9002	8.9092
		FSDT**	33.9966	24.5209	18.8566	10.5963	9.8980	8.9084
	2	Present	33.9567	24.5613	18.8022	10.6904	9.9371	8.9145
		HSDT*	33.7942	24.4204	18.8020	10.5695	9.8764	8.8938
		FSDT**	33.9881	24.5168	18.8545	10.5952	9.8970	8.9078
(-1,1)	0	Present	87.7348	78.9878	72.2869	23.3522	18.4017	9.2308
		HSDT*	86.4537	78.6141	72.2275	23.2027	18.3875	9.2100
		FSDT**	85.9468	78.4033	72.0834	22.9473	18.3902	9.2089
	1	Present	90.0425	80.8736	73.6687	23.4586	18.5717	9.2618
		HSDT*	89.1448	80.6283	73.6645	23.3907	18.5048	9.2534
		FSDT**	88.6686	80.4424	73.6307	23.1814	18.5038	9.2537
	2	Present	89.0374	80.0564	73.1598	23.0716	18.3408	9.2402
		HSDT*	88.2837	79.9839	73.1587	22.9933	18.3005	9.2387
		FSDT**	88.6336	80.4165	73.6112	23.1784	18.5024	9.2531

** (Bodaghi and Saidi, 2010); * (Mohammadi *et al.*, 2010b)

an FGM plates with different boundary conditions. For all loading conditions and boundary conditions, a close agreement between the results can be observed.

For convenience, following nondimensional critical buckling load is used in presenting the numerical results in graphical and tabular forms

$$\bar{N} = \frac{N_{cr} a^2}{E_M h^3} \quad (27)$$

The nondimensional critical buckling loads have been tabulated in Tables 4 and 5 for ceramic-FGM-metal plates under three different types of loading (uniaxial compression, biaxial compression, and compression along the x -axis and tension along the y -axis).

Table 4 The effect of fraction index p and t_{FGM}/h on nondimensional critical buckling load of square hybrid functionally graded plate whit ($a/h = 10$) under different loading conditions

t_{FGM}/h	(γ_1, γ_2)	p								
		0	0.1	0.2	0.5	1	2	5	10	∞
0	(-1,0)	7.5632	7.5632	7.5632	7.5632	7.5632	7.5632	7.5632	7.5632	7.5632
	(-1,-1)	3.7816	3.7816	3.7816	3.7816	3.7816	3.7816	3.7816	3.7816	3.7816
	(-1,1)	15.0408 ^a	15.0408 ^a	15.0408 ^a	15.0408 ^a	15.0408 ^a	15.0408 ^a	15.0408 ^a	15.0408 ^a	15.0408 ^a
0.2	(-1,0)	8.5641	8.3996	8.2626	7.9655	7.6818	7.42520	7.2150	7.1411	7.0740
	(-1,-1)	4.2820	4.2000	4.1313	3.9828	3.8409	3.7126	3.6075	3.5705	3.5370
	(-1,1)	17.095 ^a	16.7562 ^a	16.4733 ^a	15.8565 ^a	15.2614 ^a	14.7118 ^a	14.2411 ^a	14.0641 ^a	13.8888 ^a
0.4	(-1,0)	10.2454	9.8243	9.4746	8.7225	8.0275	7.4463	7.0493	6.9438	6.8707
	(-1,-1)	5.1227	4.9122	4.7373	4.3613	4.0138	3.7231	3.5247	3.4719	3.4354
	(-1,1)	20.3936 ^a	19.5482 ^a	18.8448 ^a	17.3252 ^a	15.903 ^a	14.675 ^a	13.7512 ^a	13.4502 ^a	13.1758 ^a
0.6	(-1,0)	12.7333	11.9341	11.2709	9.853	8.5702	7.5551	6.946	6.8039	6.6679
	(-1,-1)	6.3667	5.9670	5.6354	4.9265	4.2851	3.7776	3.4730	3.4019	3.3340
	(-1,1)	25.1484 ^a	23.5792 ^a	22.2746 ^a	19.47264 ^a	16.906 ^a	14.8037 ^a	13.363 ^a	12.9086 ^a	12.4435 ^a
0.8	(-1,0)	16.1289	14.8014	13.7007	11.3554	9.2608	7.6603	6.7565	6.5073	6.0209
	(-1,-1)	8.06443	7.4007	6.8503	5.6777	4.6304	3.8302	3.3782	3.2537	3.0105
	(-1,1)	31.4984 ^a	28.948 ^a	26.8271 ^a	22.2839 ^a	18.1768 ^a	14.939 ^a	12.857 ^a	12.1622 ^a	11.1671 ^a
1	(-1,0)	20.535	18.4968	16.8076	13.2165	10.0325	7.6401	6.2476	5.6339	3.4225
	(-1,-1)	10.2675	9.2484	8.4038	6.6082	5.0163	3.8201	3.1238	2.817	1.7112
	(-1,1)	39.6192 ^a	35.7739 ^a	32.5753 ^a	25.7322 ^a	19.5915 ^a	14.86 ^a	11.8583 ^a	10.5663 ^a	6.6032 ^a

^aMode for plate is (m, n) = (2, 1)

Table 5 The effect of fraction index p and side-to-thickness ratio a/h on nondimensional critical buckling load of square hybrid functionally graded plate whit ($t_{FGM}/h = 0.8$) under different loading conditions

a/h	(γ_1, γ_2)	p								
		0	0.1	0.2	0.5	1	2	5	10	∞
10	(-1,0)	16.1289	14.8014	13.7007	11.3554	9.2608	7.6603	6.7565	6.5073	6.0209
	(-1,-1)	8.0644	7.4007	6.8503	5.6777	4.6304	3.8302	3.3782	3.2537	3.0105
	(-1,1)	31.4984 ^a	28.9480 ^a	26.8271 ^a	22.2839 ^a	18.1768 ^a	14.9390 ^a	12.857 ^a	12.1622 ^a	11.1671 ^a
20	(-1,0)	16.6868	15.3012	14.154	11.717	9.5547	7.9316	7.0936	6.9043	6.4175
	(-1,-1)	8.3434	7.6506	7.0770	5.8585	4.7774	3.9658	3.5468	3.4521	3.2087
	(-1,1)	34.1729 ^a	31.3482 ^a	29.0074 ^a	24.0277 ^a	19.5946 ^a	16.2366 ^a	14.4185 ^a	13.958 ^a	12.9833 ^a
30	(-1,0)	16.7944	15.3975	14.2413	11.7865	9.6113	7.984	7.1599	6.9832	6.4968
	(-1,-1)	8.3972	7.6988	7.1206	5.8933	4.8056	3.9920	3.5799	3.4916	3.2484
	(-1,1)	34.7196 ^a	31.8377 ^a	29.4513 ^a	24.3816 ^a	19.8823 ^a	16.5026 ^a	14.7511 ^a	14.3514 ^a	13.3371 ^a
40	(-1,0)	16.8324	15.4315	14.2721	11.8111	9.6312	8.0025	7.1833	7.0113	6.5250
	(-1,-1)	8.4162	7.7158	7.1360	5.9055	4.8156	4.0013	3.5917	3.5057	3.2625
	(-1,1)	34.9151 ^a	32.0127 ^a	29.61 ^a	24.508 ^a	19.985 ^a	16.5978 ^a	14.8713 ^a	14.4945 ^a	13.4808 ^a
50	(-1,0)	16.8501	15.4473	14.2864	11.8225	9.6405	8.0111	7.1943	7.0244	6.5381
	(-1,-1)	8.425	7.7237	7.1432	5.9112	4.8202	4.0056	3.5971	3.5122	3.2691
	(-1,1)	35.0064 ^a	32.0943 ^a	29.684 ^a	24.5669 ^a	20.033 ^a	16.6422 ^a	14.9275 ^a	14.5618 ^a	13.5408 ^a

^aMode for plate is (m, n) = (2, 1)

Table 4 shows the influence of FGM layer thickness t_{FGM} on the mechanical buckling behavior for the hybrid functionally graded plate of which the all-ceramic layer thickness $t_{Ceramic}$ is equal to the all-metal layer thickness t_{Metal} . As can be seen, the nondimensional critical buckling load decreases with the increase in volume fraction index, whatever the type of loading is. A small volume fraction index p indicates that the ceramic is the dominant constituent in the hybrid FGM. Thus, the increase in the critical buckling load of a functionally graded plate could be attributed to the ceramic property. As expected, the critical buckling load will be maximum for the pure-ceramic plate ($t_{FGM} = h, p = 0$) and be minimum for the pure-metal plate ($t_{FGM} = h, p = \infty$). As volume fraction index equals to one ($p = 1$), the change of the critical buckling load of the hybrid functionally graded plate is not significantly affected by the increasing thickness of middle FGM layer of hybrid functionally graded plate. It can be observed that the critical buckling load increases with the increasing thickness of an FGM layer (t_{FGM}) for hybrid functionally graded plates with a lower volume fraction index ($p < 1$). However, for functionally graded plates with a high volume fraction index ($p > 1$), the thickness of an FGM layer produces a reverse effect. The results indicate that the critical buckling load of functionally graded plates is enlarged by the ceramic constituent.

The effects of ceramic volume fraction p and thickness ratio a/h on the nondimensional critical buckling load of hybrid functionally graded plates are presented in Table 5. It is apparent from the data that, with the increase of p and the decrease of a/h , the nondimensional critical buckling load of hybrid functionally graded plate drops significantly.

In Fig. 3, the nondimensional critical buckling load of square hybrid functionally graded plate is plotted versus the volume fraction index p for three different types of loading. This figure shows that the nondimensional critical buckling load decreases significantly with increasing the power of FGM p . This is due to the fact that increasing the power of FGM increases the volume fraction of metal. Also, the variation of the nondimensional critical buckling load for the power of FGM more than 2 is small.

The effect of the FGM layer thickness on the nondimensional critical buckling load of hybrid functionally graded plate under three different types of loading is shown in Fig. 4. It can be observed that the nondimensional critical buckling load increases with the increasing thickness of an FGM layer

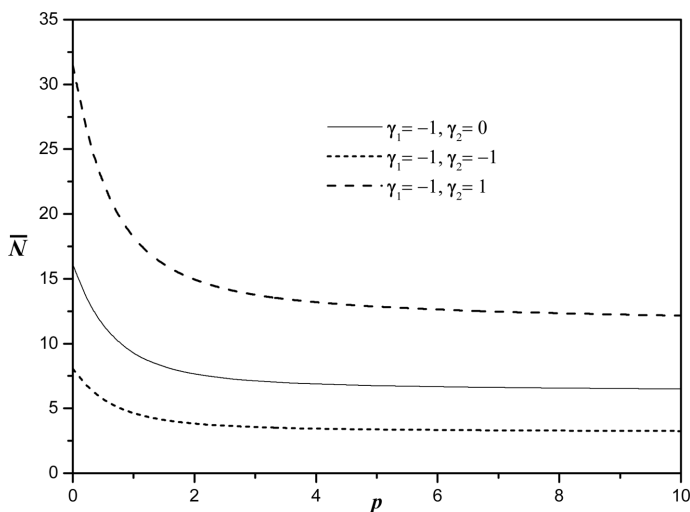


Fig. 3 The nondimensional critical buckling load of square hybrid functionally graded plate versus the power of FGM for three different types of loading with $a/h = 10$ and $t_{FGM}/h = 0.8$

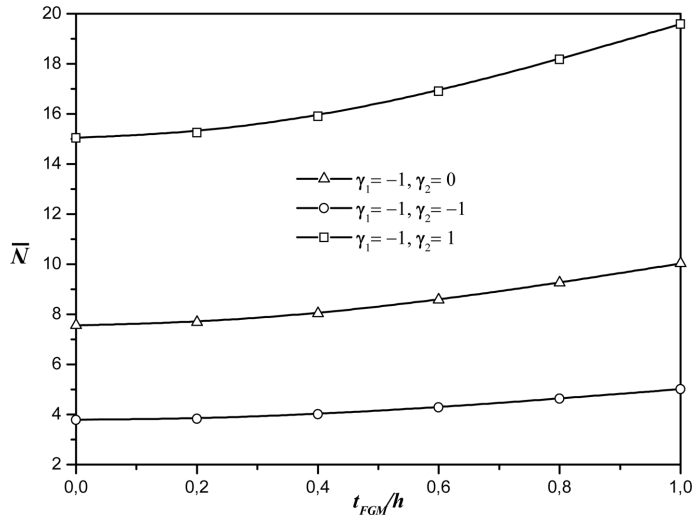


Fig. 4 The nondimensional critical buckling load of square hybrid functionally graded plate versus t_{FGM}/h for three different types of loading with $a/h = 10$ and $p = 1$

(t_{FGM}) for hybrid functionally graded plates with volume fraction index $p = 1$. Moreover, it can be observed from Figs. 3 and 4 that the critical buckling load of hybrid functionally graded plate under uniaxial compression ($\gamma_1 = -1, \gamma_2 = 0$) is greater than that under biaxial compression ($\gamma_1 = -1, \gamma_2 = -1$) and less than that under compression along the x-axis and tension along the y-axis ($\gamma_1 = -1, \gamma_2 = 1$).

Figs. 5 and 6 show the variation of nondimensional critical buckling load of square hybrid functionally graded plate versus the modulus ratio E_C/E_M of FGM (i.e., different ceramic-metal

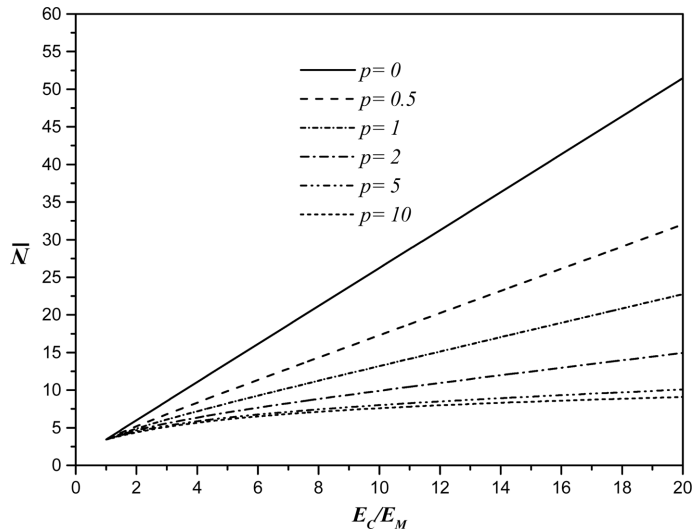


Fig. 5 The effect of modulus ratio and the power of FGM ($p = 1$) on nondimensional critical buckling load of square hybrid plate ($a/h = 10$) under uniaxial compression along the x-axis ($\gamma_1 = -1, \gamma_2 = 0$) with $t_{FGM}/h = 0.8$

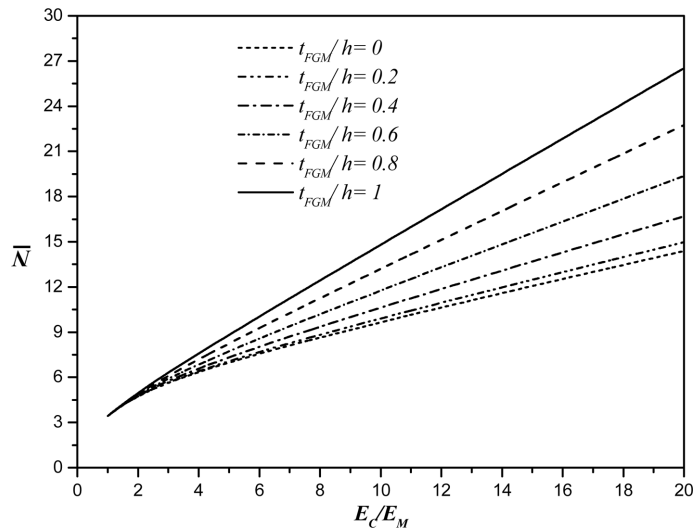


Fig. 6 The effect of modulus ratio and the FGM layer thickness (t_{FGM}/h) on nondimensional critical buckling load of square hybrid plate ($a/h = 10$) under uniaxial compression along the x-axis ($\gamma_1 = -1$, $\gamma_2 = 0$) with $p = 1$

mixtures) for different powers of FGM and t_{FGM}/h , respectively. The side-to-thickness ratio a/h is assumed to be 10. It is observed that the critical buckling load increases as the metal-to-ceramic modulus ratio increases and decreases as the power of FGM increases. However, the critical buckling load increases with the FGM layer thickness (t_{FGM}/h) for $p = 1$.

6. Conclusions

In this research work, buckling analysis of thick ceramic-FGM-metal plates has been presented. Based on the new four variable refined plate theory, the equilibrium and stability equations of hybrid functionally graded plates have been derived. The number of unknown functions involved in the theory is only four. Even in higher shear deformation theory (HSDT), five unknown functions are involved. The accuracy and efficiency of the present theory have been demonstrated for buckling analysis of simply supported ceramic-FGM-metal plates. It can be concluded that the present theory is not only accurate but also efficient in predicting the critical buckling loads of hybrid functionally graded plate compared to other shear deformation plate theories such as HSDT. The presented formulations and results will be a useful benchmark for researchers to check out their analytical and numerical methods and also for engineering designers deal with analyzing functionally graded plates in the future.

References

- Abrate, S. (2008), "Functionally graded plates behave like homogeneous plates", *Composites Part B: Engineering*, **39**(1), 151-158.
- Bodaghi, M., Saidi, A. (2010), "Levy-type solution for buckling analysis of thick functionally graded rectangular

- plates based on the higher-order shear deformation plate theory”, *Appl. Math. Model.*, **34(11)**, 3659-3673.
- Bouazza, M., Tounsi, A., Adda-Bedia, E.A., Megueni, A. (2010), “Thermoelastic stability analysis of functionally graded plates: An analytical approach”, *Comput. Mater. Sci.*, **49(4)**, 865-870.
- Chehel Amirani, M., Khalili, S.M.R., Nemati, N. (2009), “Free vibration analysis of sandwich beam with FG core using the element free Galerkin method” *Compos. Struct.*, **90(3)**, 373-379.
- Chi, S., Chung, Y. (2006a), “Mechanical behavior of functionally graded material plates under transverse load - Part I: Analysis.” *Int. J. Sol. Struc.*, **43(13)**, 3657-3674.
- Chi, S., Chung, Y. (2006b), “Mechanical behavior of functionally graded material plates under transverse load - Part II: Numerical results”, *Int. J. Sol. Struc.*, **43(13)**, 3675-3691.
- Delale, F., Erdogan, F. (1983), “The crack problem for a nonhomogeneous plane”, *J. of Appl. Mech.*, **50**, 609-614.
- Feldman, E., Aboudi, J. (1997), “Buckling analysis of functionally graded plates subjected to uniaxial loading”, *Compos. Struct.*, **38(1-4)**, 29-36.
- Gibson, LJ, Ashby, MF, Karam, GN., Wegst, U., Shercliff, HR. (1995), “Mechanical properties of natural materials. II. Microstructures for mechanical efficiency”, *Proc Roy Soc Lond A*, **450(1938)**, 141-162.
- Hill, R. (1965), “A self-consistent mechanics of composite materials”, *J Mech Phys Solids*, **13(4)**, 213-222.
- Javaheri, R., Eslami, M. (2002), “Buckling of functionally graded plates under in-plane compressive loading”, *J. Appl. Math. Mech.*, **82(4)**, 277-283.
- Levinson, M. (1980), “An accurate simple theory of the statics and dynamics of elastic plates”, *Mech Res Commun*, **7(6)**, 343-350.
- Mahdavian, M. (2009), “Buckling analysis of simply-supported functionally graded rectangular plates under non-uniform In-plane compressive loading”, *J. Solid Mech.*, **1(3)**, 213-225.
- Mindlin, RD. (1951), “Influence of rotary inertia and shear on flexural motions of isotropic, elastic plates”, *J. Appl. Mech*, **18(1)**, 31-38.
- Mohammadi, M., Saidi, A.R., Jomehzadeh, E. (2010a), “Levy solution for buckling analysis of functionally graded rectangular plates”, *Appl. Compos. Mater.*, **17(2)**, 81-93.
- Mohammadi, M., Saidi, A.R., Jomehzadeh, E. (2010b), “A novel analytical approach for the buckling analysis of moderately thick functionally graded rectangular plates with two simply-supported opposite edges”, *Proc. Inst. Mech. Engrs. Part C J. Mech. Eng. Sci.*, **224(9)**, 1831-1841.
- Mori, T., Tanaka, K. (1973), “Average stress in matrix and average elastic energy of materials with misfitting inclusions”, *Acta Metall*, **2**, 1571-1574.
- Narita, Y. (2000), “Combinations for the free vibration behaviors of anisotropic rectangular plates under general edge conditions”, *J. Appl. Mech*, **67(3)**, 568-573.
- Reddy, J. (2004), “Mechanics of laminated composite plates and shells: theory and analysis”, CRC.
- Reddy, J.N. (1984), “A simple higher order theory for laminated composite plates”, *J. Appl. Mech*, **51**, 745-752.
- Reissner, E. (1945), “The effect of transverse shear deformation on the bending of elastic plates”, *J Appl Mech-T ASME*, **12(2)**, 69-77.
- Shariat, B., Eslami, M. (2005), “Buckling of functionally graded plates under in plane compressive loading based on the first order plate theory”, *Proceeding of the Fifth International Conference on Composite Science and Technology*; American University of Sharjah, United Arab Emirates.
- Yang, J., Liew, K., Kitipornchai, S. (2005), “Second-order statistics of the elastic buckling of functionally graded rectangular plates”, *Compos. Sci. Technol.*, **65(7-8)**, 1165-1175.
- Zhao, X., Lee, Y.Y., Liew, K.M. (2009), “Mechanical and thermal buckling analysis of functionally graded plates”, *Compos. Struct.*, **90(2)**, 161-171.